Regular Article

ANALYTICAL
AND BIOANALYTICAL
CHEMISTRY
RESEARCH

Published by the
Iranian Chemical Society

***Anal. Bioanal. Chem. Res.**, Vol. 10, No. 1, 87-96, January 2023.*

Polythiophene Imprinted CeO_2 Fluorescent Probe for Lead Detection in Tab Water Samples

Abdu Hussen Ali*

Department of Chemistry, College of Natural and Computational Sciences, Mekdela Amba University; P. O. Box: 32, Tuluawliya, Ethiopia

(Received 23 July 2022, Accepted 10 October 2022)

The development of real-time, highly sensitive, and selective, simple techniques for the detection of toxic Pb^{2+} in water was challenged. However, in this study, a highly efficient fluorescent probe based on polythiophene imprinted CeO_2 nanocomposite for selective detection of Pb^{2+} ion was developed by polymerization method. The developed fluorescent probe was characterized by using powder X-ray diffraction (XRD), Fourier-Transform Infrared spectroscopy (FT-IR), and Scanning Electron Microscope (SEM). Upon binding to the imprinted binding sites PT/CeO_2 the Pb^{2+} interacts with the molecular orbital and their fluorescence is quenched *via* reverse photoinduced electron transfer which results in qualitative and quantitative detection. The factor affecting the detection system such as pH and concentration are optimized. Additionally, the PT/CeO_2 fluorescent sensor exhibits high sensitivity with a Stern Volmer quenching (KSV) value of 6.39×10^3 M^{-1}. The practical application of the sensor was also tested by spiking with different concentrations of Pb^{2+} ion solutions on tab water samples. The result indicates a good linear relation between F_O/F and the spiked concentrations with the coefficient of regression $R^2 = 0.99$ (n = 3) and also confirms that the found values are agreed well with the spiked amount. The obtained amounts of lead metal ion concentrations in tap water were 15.39 μM which exceeded the allowable limit as stated by WHO.

Keywords: Imprinted, Fluorescence sensor, Polythiophene, Quenching, Toxic heavy metal

INTRODUCTION

Heavy metal ions pollution and its effects on human life are one of the most studied environmental issues in recent years. Today's world faces alarming challenges in the rising demand for clean drinking water, and conditions are particularly bad in developing countries [1]. This is due to environmental pollution by heavy metals can occur in many different ways, either directly or indirectly. Soils and water are contaminated by material from the air or by direct deposition of pollutants. Heavy metals (HM), with high atomic numbers and much higher density than water, are present in the environment naturally. Their contamination of the environment is due to artificial industrial operations and also due to other causes such as the dissolution of metals (through metal corrosion), and heavy metals leaching [2]. Moreover, heavy metals are indestructible and have toxic effects on living organisms, especially at high concentrations [3]. In general, the toxicity of metal ions to mammalian systems is due to the chemical reactivity of the ions with cellular structural proteins, enzymes, and membrane systems. The target organs of specific metal toxicities are usually those organs that accumulate the highest concentrations of the metal *in vivo*.

Heavy metal ions refer to metallic elements, which include such as iron, cobalt, copper, manganese, molybdenum, zinc, mercury, plutonium, and lead. Heavy metals are dangerous because they tend to bioaccumulate. Among them, lead is highly toxic and can affect every organ and system in the body. The main sources of lead exposure

*Corresponding author. E-mail: abdelmelik9@gmail.com

are lead-based paints, gasoline, cosmetics, toys, household dust, contaminated soil, and industrial emissions [4]. Lead poisoning was considered to be a classic disease and the signs that were seen in children and adults were mainly pertaining to the central nervous system and the gastrointestinal tract [5]. This lead poisoning can also occur from drinking water. The pipes that carry the water may be made of lead and its compounds which can contaminate the water [6]. Its distribution in the body initially depends on the blood flow into various tissues and almost 95% of lead is deposited in the form of insoluble phosphate in skeletal bones. Chronic exposure to lead metal ion can result in mental retardation, birth defects, psychosis, autism, allergies, dyslexia, weight loss, hyperactivity, paralysis, muscular weakness, brain damage, and kidney damage and may even cause death [7].

There exist several traditional methods that characterize the presence of heavy metals in waters, qualitatively and quantitatively. Atomic Absorption Spectroscopy (AAS), Inductively Coupled Plasma-Mass Spectrometry (ICP-MS), and Inductively Coupled Plasma/Atomic Emission Spectrometry (ICP-AES) are a few of the methods that can be applied to detect and measure the presence of heavy metals in water samples [8]. Even though those methods have great sensitivity and selectivity, however, there exist several disadvantages such as the high cost of the instruments, long sample preparations time, the requirement for calibration standards, and the requirement for well-trained personnel for the operation.

Fluorescent probes have concerned great attention due to their high accuracy, high sensitivity, fast analysis, and simplicity. To date, various fluorescent probes including fluorescent metal nanoparticles, organic dyes, and semiconductor quantum dots (QD) are exceptional examples of these applications. Especially in the field of environmental monitoring, the application of nanoparticles (NPs) based fluorescent probes are being utilized as functional probes for analyzing toxins, metal ions, and inorganic and organic pollutants [9]. NPs, usually with a size between 1 and 100 nm, display unique properties, mainly due to the strong physical confinement of electrons or holes in the NPs at the nanoscale. From a sensing perspective, the small size of NPs gives them large surface-to-volume ratios, which lead to rapid responses and high sensitivity.

Fluorescent sensors based on decorated noble metal nanoparticles (NPs) have also attracted great attention for their convenience of simple operation in recent years. From many metallic nanoparticles, cerium oxide with different valence states has been explored for various applications such as electrical, electronic, catalytic, adsorption, optical, functional materials, energy storage, and sensing properties [10,11]. CeO_2 has a positive prospect on luminescence properties due to its capacity for light absorption and the ability to emit through $O^{2-} \rightarrow Ce^{4+}$ transition. Nanoceria is optically active and can develop unique color patterns depending upon specific interactions at their surface [12]. The optical properties of cerium oxide and gold-ceria nanoparticles; and their uses for dissolved oxygen and lead metal ion detection based on fluorescence quenching were also reported [13].

The improvement of the fluorescent detection mechanism for pollutants became achieved when supporting the metallic nanomaterial by conducting polymers, because of its mechanical flexibility, large surface area, and high optical properties. The semiconductive nature of these conducting polymers gives them very useful optical and optoelectronic properties. This sensitivity arises from the collective optical and conducting properties of the CP. These polymers are extremely sensitive to minor external structural perturbations or electron density changes within the polymer, due to their ability to self-amplify their fluorescence quenching response upon perturbation of the electronic network upon binding of analytes. Depending on the system, a CP can exhibit a strong luminescence, the luminescence efficiency is related to the delocalization and polarization of the electronic structure [14]. Among different conducting polymers, Polythiophene is one of the most valuable types of conducting polymers that may be easily modified to afford a variety of useful electrical and physical properties such as solubility, electrical conductivity, mobility, and others. Polythiophene has been widely used in environmentally and thermally stable conjugated polymer materials rather than other conducting materials, such as chemical and optical sensors, light emitting diodes and displays, photovoltaic devices, molecular devices, DNA detection, polymer electronic interconnects and transistors [15,16].

This study focuses on developing noble sensing material polythiophene imprinted CeO_2 for the detection of highly toxic lead metal in water. PT/CeO_2 was successively

fabricated by the polymerization method. The properties of polythiophenes can be selectively engineered through planarization of the backbone and assembly of the backbone in the form of π stacks lead to better materials and enhanced device performance in almost every category, ranging from optical property to stability.

EXPERIMENTAL

Materials

Reagents were of analytical grade or the highest commercially available purity and were used as received. Cerium nitrate hexahydrate (India, 99%), sodium dihydrogen phosphate (98%), disodium hydrogen phosphate (98%), hydrochloric acid (England, 37%), ethanol (absolute grade, 99%), ammonia, copper sulfate, lead sulfate, ferric chloride, chloroform, thiophene, sodium chloride, sodium hydroxide (BDH England, 98 %), magnesium sulfate (Fisher Scientific, 99%), calcium sulfate, nickel nitrate, cobalt nitrate, ferrous sulfate (BDG England, 99%), chromium sulfate, cadmium nitrate, and zinc chloride were used without purification.

Synthesis of Nanocomposites

Preparation of CeO_2 nanoparticle. The cerium oxide ultrafine nanoparticle was prepared by a precipitation method [17]. An aqueous solution of 0.1 M (4.334 g in 100 ml) of cerium nitrate hexahydrate $Ce(NO_3)_3.6H_2O$ in deionized water was prepared and stirred for 30 min. The clear solution was precipitated by the dropwise addition of aqueous NH_4OH solution with continuous stirring until precipitation gets completed. The stirring was continued for another 2 h and the reaction condition was then maintained at pH = 10. The reaction mixture was then stirred for 12 h to complete the precipitation process. The mixture was aged for 12 h. The resulting yellow-colored slurry was decanted, and the precipitate was filtered and washed three times with deionized water and ethanol. The clean precipitate was oven dried at 140 °C for 12 h and calcined at 500 °C for 3 h to promote the crystallization.

Synthesis of polythiophene (PT). The synthesis of PT is carried out with some modifications described in the literature. 1.0 g Thiophene in 10 ml of chloroform and 8.0 g of the oxidizing agent $FeCl_3$ in 50 ml of chloroform was prepared. The two solutions are mixed and stirred for 12 h at a temperature of 5 ºC. Polymerization proceeded for 5.5 h. After the filtration and washing, the solid was re-suspended and washed using Milli-Q water until a pH 7 was reached. The PT solid was dried under vacuum at 60 ºC for 24 h [18].

Synthesis of polythiophene (PT)/CeO_2. A typical polymerization method was adopted for the polymerization of thiophene in the presence of CeO_2 nanoparticles. Briefly, 0.2 g of CeO_2 was added to 50 mL chloroform and thoroughly mixed. Later, 8.0 g of the oxidizing agent $FeCl_3$ was added to the mixture and stirred for 30 min. 1.0 g of thiophene monomer was added to the solution and left under agitation for 12 h at 5 ºC. Polymerization proceeded for 5.5 h. Then the solution was filtered and washed with Milli-Q water. The precipitate was re-suspended in 100 ml of 1 M HCl and stirred for 2 h. After filtration, the solid was rinsed with a 1 M HCl solution until the filtrate was colorless. Following the rinsing, the composite was then washed with Milli-Q water until a pH 7 was reached. The PT/CeO_2 composites were then dried under vacuum conditions at a temperature of 40 ºC for 24 h.

Characterization of the Synthesized Nanocomposites

The fluorescent emission properties were determined using an RF-5301PC spectrofluorometer (SHIMADZU, Japan) equipped with a xenon discharge lamp. The surface morphology was studied by scanning electron microscopy (SEM) using a flexsem1000. The crystalline phases and the crystallite sizes were determined using powder X-ray diffraction (XRD) with X'Pert Pro PANalytical with CuKα radiation (λ = 1.5405 Å). The data were registered with 2θ steps of 0.02° and accumulation times of 20 s. FT-IR spectra (Spectrum 65, PerkinElmer) in the range 4000-400 cm^{-1} using KBr pellets were used to assign functional groups of as-synthesized PT/CeO_2.

Preparation of Buffers

The 0.1 M phosphate buffer was prepared by weighing approximately 0.8 g of $NaH_2PO_4.2H_2O$ and 6.5 g of Na_2HPO_4 and dissolving them in water into a 500 ml volumetric flask. It was adjusted using 0.1 M HCl or 0.1 M NaOH to the desired pH. The buffer solution was stored in a fridge at 4 °C [19].

Fluorescence Detection of Lead Ions

For fluorescence detection of lead metal ions, 2 ml of PBS (0.1 M, pH 7.4) was added into 0.02 g of the PT/CeO_2 nanocomposite, followed by the addition of different molar concentrations of Pb^{2+} ion, and sonicated. After a reaction time of 5 min at room temperature, 100 µl of the solution was taken into a cuvette and finally, the excitation and emission spectra were recorded using fluorescence spectroscopy.

To quantify the Pb^{2+} induced quenching process, the Stern-Volmer quenching constant K_{SV} was calculated by the Stern-Volmer equation:

$$I_O/I = 1 + K_{SV}[Q] \quad (1)$$

Where I_O and I are the fluorescence intensities of the fluorescent sensor in the absence and presence of lead metal ions, respectively, K_{SV} is the Stern-Volmer constant, and (Q) is the molar concentration of the lead metal ion.

Optimization of Parameters

The Effect of pH. Commonly, the pH of a solution can affect the sensitivity and selectivity of a detection. The effect of pH (2-12) of PBS on the PT/CeO_2 fluorescent probe in the presence of lead ion solution was tested.

The Effect of Concentration. To investigate this effect, 2 ml of PBS (0.1 M, pH = 7) was added to 0.02 g of the PT/CeO_2 nanocomposite, followed by the addition of 50, 150, 200, 250, 300, 350, 450, and 500 µM of lead solution and sonicated. After a reaction time of 5 min at room temperature, 100 µl of the solution was taken into a cuvette and finally, the excitation and emission spectra were recorded using fluorescence spectroscopy.

Reproducibility and Stability Tests

The reproducibility of the PT/CeO_2 as the fluorescent sensor was investigated at three repetitions on three batches of the PT/CeO_2. A calibrat ion graph was plotted for the mean of F_O/F, (F_O and F represented the fluorescence intensity of the sensor without and with lead) *vs*. lead concentration, which a linear range was then determined. The limit of detection was calculated using the following formula;

$$LOD = \frac{3\,x\,SD}{K_{SV}} \quad (2)$$

Where LOD is the limit of detection, SD is the standard deviation from the linearity of a graph and K_{SV} is the Stern-Volmer constant calculated from the graph [20].

Selectivity of the Sensor

The Zn^{2+}, Ni^{2+}, Co^{2+}, Mg^{2+}, Ca^{2+}, Cu^{2+}, Cd^{2+}, Cr^{2+} and Fe^{2+} ions were used to investigate selectivity for Pb^{2+} ion of PT/CeO_2 fluorescent probe. The concentration of each metal ion was 500 µM. The same detection conditions and approach were used as mentioned above.

Recovery Test and Real Samples Analysis

Tap water samples were collected from the Tuluawliya, Legambo Woreda. The tap water samples were spiked with different concentrations of lead(II) solutions. Typically, 300 µl of sample solutions was taken and added to PT/CeO_2 nanocomposite in 2 ml PBS (pH = 6). Finally, fluorescence emission spectra were recorded after a reaction time of 5 min at room temperature.

The mean percentage recoveries for the lead ions were calculated using the following equation:

$$\text{Percentage recovery} = \frac{CE}{CM} \times 100 \quad (3)$$

Where CE is the experimental concentrations determined from the calibration curve and CM is the spiked concentrations.

RESULTS AND DISCUSSION

Characterization of the Synthesized Nanomaterial

FT-IR Analysis. The FT-IR spectrum in the mid-infrared region is the feature of a particular compound that gives information about the functional groups. It can be seen in Fig. 1, pure polythiophene (PT) shows the presence of characteristic absorption bands at 3.440 cm^{-1} assigned for O–H stretching, 1697.17 and 1469 cm^{-1} assigned for C=C asymmetric and symmetric stretching vibration of thiophene ring respectively [21]. The peak 750 cm^{-1} was assigned for the C-S bending vibration of polythiophene which confirms the successful polymerization of thiophene monomer and the formation of polythiophene. The bare CeO_2 shows a characteristic band at 3434 cm^{-1} corresponding to the O-H

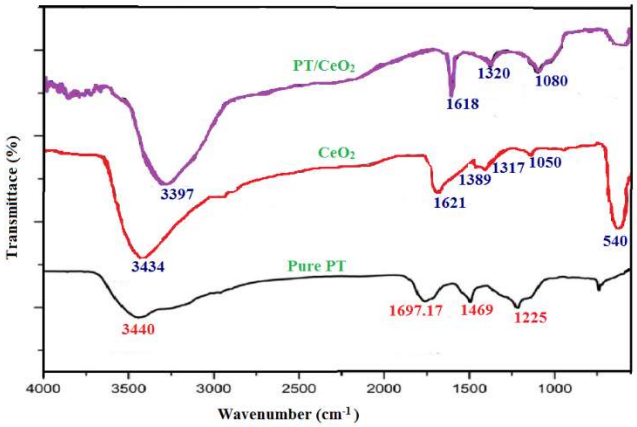

Fig. 1. FT-IR spectra of PT/CeO_2 nanocomposite.

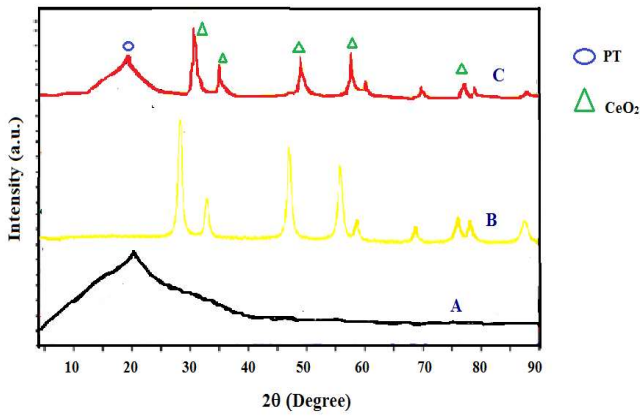

Fig. 2. XRD patterns of the nanocomposites Polythiophene (PT), B) CeO_2, C) PT/CeO_2).

stretching vibration, 1622.55 cm^{-1} assign for -OH scissor bending, which originated from physically absorbed water molecules or surface [22]. The FT-IR spectrum contains two characteristic absorption bands at 1389 and 1050 cm^{-1}, which are attributed to Ce–O bonds [10].

In the case of polythiophene/CeO_2, the peaks exhibited similar patterns of the two pure nanoparticles, however, peak shifts observed that are due to upon immobilization of the nanocomposite onto the polymer support. Accordingly, such as 3397 cm^{-1} is assigned for O–H stretching, and 1618 cm^{-1} is assigned for C=C stretching vibration of the thiophene ring which indicates the presence of polythiophene. The band at 1080 cm^{-1}, which are attributed to Ce–O bonds. The spectrum confirms that a strong covalent bond is formed between CeO_2 and the coplanar conformation of polythiophene.

XRD Analysis. The crystal structure and crystallinity of nano-material is a very important characteristic because it eventually affects many physical properties. XRD gives information about the crystal structures and identifies the phase of the materials, atomic spacing, and unit cell dimensions of crystalline material. Therefore, the crystal structure of the as-synthesized composites was studied by powder X-ray diffraction (XRD), as shown in figure 2B. The apparent peaks for CeO_2 are observed at 2θ values of 28.6°, 33.1°, 47.5°, 56.3°, 59.2°, 69.4°, 76.7°, 79.09° and 88.44° corresponding to the (111), (200), (220), (311), (222), (400), (313), (402) and (422) crystal planes of cubic crystalline phases respectively [JCPDS: 96-434-3162]. The general feature of the XRD patterns of CeO_2 shows the presence of strong and sharp peaks, which indicate that the produced nanoparticles are fine crystalline. For pure polythiophene (PT), Fig. 2A shows a significant peak at 2θ = 22.53°, which represents the characteristic conducting semi-amorphous structure of polythiophene. This work is confirmed by other findings [23].

The XRD pattern of PT/CeO_2 composites, as Figu.2C shows the existence of both polythiophene and CeO_2. The existence of CeO_2 nanoparticles in the polythiophene matrix resulted in disordered stacking of the nanocomposite. Consequently, the diffraction peak of PT/CeO_2 slightly shifted compared to the pure nanoparticle, which may be attributed to the crystal lattice distortion in PT owing to the relatively strong interaction between the CeO_2. The diffraction peak is observed at 2θ values of 23.1° ascribed to PT and 30.5°, 35.89°, 47.5° and 57.1° assigned to the (111), (200), (220), and (311) plane is due to cubic CeO_2. The crystallinity of the composite is caused by the crystalline structure of CeO_2.

Scanning electron microscopy (SEM) analysis. The scanning electron microscopy shows the surface morphology of CeO_2 described in Fig. 3A, the result indicates nearly spherical morphology. It can be seen in Fig. 3B, it is apparent PT (polythiophene) nanoparticles have a film porous structure that was clumped together as clusters, a type

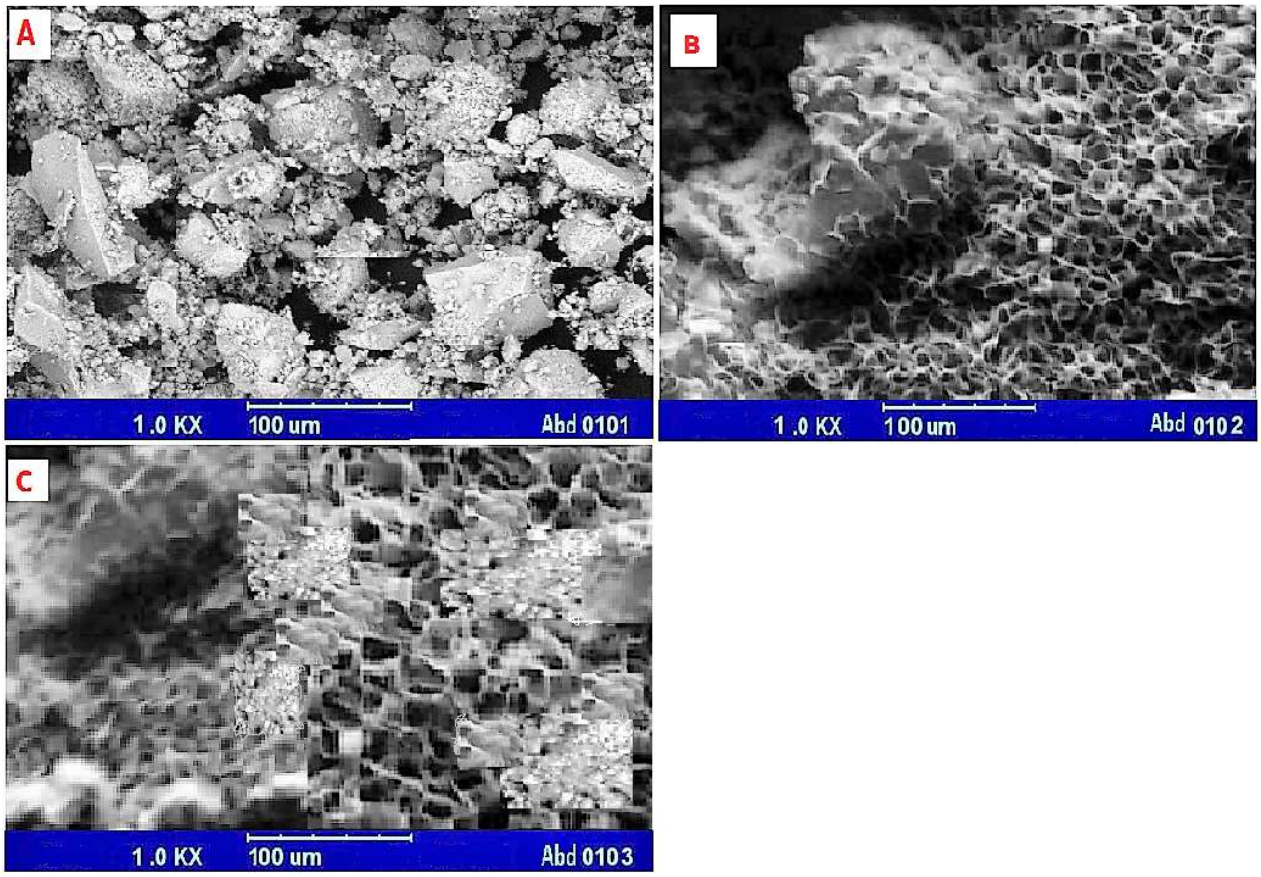

Fig. 3. Typical SEM image of (A) Polythiophene (PT), B) CeO_2, C) PT/CeO_2).

formation of PT crystals presented. Although the PT images show a granular and uniform structure, with a repetitive pattern. The surface morphologies of the as-synthesized PT/CeO_2 nanocomposite, as in Fig. 3C described the CeO_2 are nobbled on the surface of porous polythiophene polymer. Furthermore, the different structures present in the PT/CeO_2 composites from bare nanoparticles validate the formation of new materials.

Mechanism of PT/CeO_2 Fluorescent Probe for Detection of Lead Ion

The emission spectra were monitored at excitation wavelengths of 320 nm and PT/CeO_2 sensor was important for the effective sensing of toxic Pb^{2+} ion. The result indicated that Pb^{2+} can effectively quench the fluorescence intensities of PT/CeO_2 fluorescent probe due to an empty p shell, hence electron is transferred. These indicate the reverse photo-induced electron transfer mechanism involving electron donation from the excited PT/CeO_2 part to the Pb^{2+} ion resulting in no fluorescence being observed (quenching) [24]. It was also suggested that PT/CeO_2 and Pb^{2+} form a strong bond with the interaction site in (Pb–S) and (Pb–O) illustrating static quenching from the formation of a stable non-fluorescent complex. Consequently, the fluorescence intensity is significantly quenched.

Over this, an orbital of Pb^{2+} could have energy between that of the HOMO and that of the LUMO of the PT/CeO_2 probe. When this "alien" orbital is full (S and O donor group), a PET from this full orbital to the HOMO of the PT/CeO_2 can take place. The electron transfer from the LUMO of PT/CeO_2 to the Pb^{2+} orbital retrieves the stable ground state. Next this sequence, fluorescence quenching occurs because the transition from the excited to the ground state takes place following a non-radiative path as described in Fig. 4. This

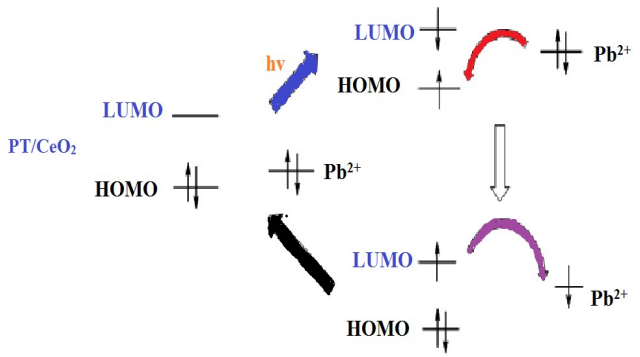

Fig. 4. Fluorescent recognition of Pb^{2+} by PT/CeO_2.

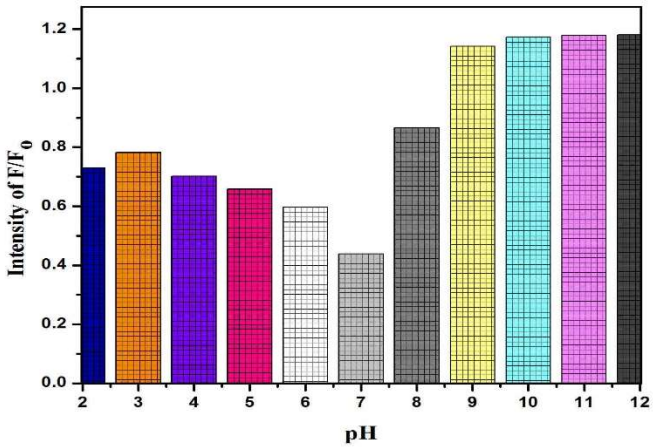

Fig. 5. Fluorescence restoration of the PT/CeO_2 with different pH solutions (0.1 M PBS). F and F_0 are the fluorescence intensities of PT/CeO_2 in the presence and absence of Pb^{2+}, respectively.

process results in a decrease in the emission intensity.

Optimization of Experimental Conditions of PT/CeO_2 Probe

To evaluate the sensitivity of the proposed material, the experimental conditions were optimized including the pH of the buffer solution and the concentration of the lead metal ion.

Influence of pH. The effect of pH on fluorescence response was carried out from pH 2-12. The influence of pH on the quenching emission intensity of PT/CeO_2 by Pb^{2+} is illustrated in Fig. 5. The relative intensity ratio values decrease on going from pH 2 to pH 6. This is due to a lower pH both the interaction sites on the sensor and the Pb^{2+} are fully protonated. Therefore, the complexation of Pb^{2+} was delayed resulting in a low quenching efficiency. As the pH increased from 7, the fluorescence intensity significantly decreased due to the high quenching efficiency, and maximum quenching was observed at pH 7. This is due to the deprotonation of the interaction site, which increases the covalent bond strength between the PT/CeO_2 and Pb^{2+}. The pH further increases pH greater than 8, competitive lead hydroxide is formed, it resulted in a distinct increase in fluorescence intensity resulting in a poor interaction with the PT/CeO_2 probe. Hence, pH 7 is recommended as the optimal pH value for further detection.

Concentration of Pb^{2+}. The sensitivity of the emission behavior of the ultrasmall particles has been exploited for the determination of Pb^{2+} in an aqueous solution. The changes in emission spectra (quenching) of the developed probe upon

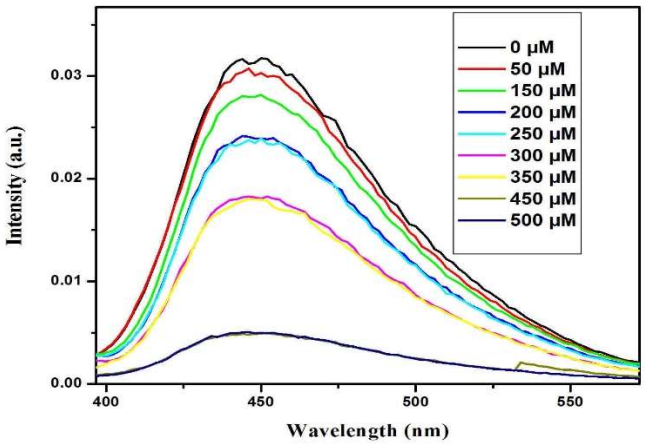

Fig. 6. The emission spectrum of PT/CeO_2 upon the addition of Pb^{2+} with various concentrations.

the addition of different concentrations of Pb^{2+} as designated in Fig. 6. As described in the mechanism above (section 3.2) this is due to the Pb^{2+} forming a covalent bond with the PT/CeO_2, so resulting in photoinduced electron transfers (PET). The emission is gradually quenched with an increase in the concentration of these Pb^{2+} in an aqueous solution from 50 to 500 µM, and the fluorescence intensity, therefore, decreases linearly.

The Sensitivity of PT/CeO_2 Probe

The fluorescence intensity of PT/CeO_2 was found to be such that quenching and the Stern-Volmer fluorescence intensity ratio (F_O/F) show a linear diminish with the increasing the Pb^{2+} concentration from 50 µM to 500 µM in a phosphate buffered solution (PBS, 0.1M, pH = 7). The result showed that the Pb^{2+} concentration is inversely proportional to fluorescence intensity, and gave a good linear change in the Stern-Volmer fluorescence emission intensity ratio. The quenching efficiency was determined using a Stern-Volmer equation (Eq. (1)). From the calibration curve, as described in Fig. 7, there is a linear dependence of the emission intensity on the concentration of Pb^{2+} with the coefficients of regression of $R^2 = 0.98$. The calculated K_{SV} value for the PT/CeO_2 fluorescent probe for the detection of Pb^{2+} was found to be $6.39 \times 10^{3}\ M^{-1}$. The proposed PT/$CeO_2$ fluorescent nanocomposite is more sensitive when compared with other findings.

The limit of detection was determined by performing a reproducibility test at three repetitions. Therefore, the LOD of the PT/CeO_2 for the Pb^{2+} is determined from the standard deviation of the response at the intercept of the regression line and the value of the K_{SV} (Eq. (2)). The limit of detection of the proposed probe for Pb^{2+} was found to be 9.17×10^{-5} M.

Selectivity of PT/CeO_2 for Pb^{2+}

The detection of Pb^{2+} is usually accompanied by severe interferences of various ionic species. The fluorescence features of the developed probe were tested by other competitive metal cations rather than the target ion, including Zn^{2+}, Ni^{2+}, Co^{2+}, Mg^{2+}, Ca^{2+}, Cu^{2+}, Cd^{2+}, Cr^{2+}, and Fe^{2+} ions under the same conditions. The selectivity test was performed by adding metal salt solutions to the PT/CeO_2 in PBS and mixing them to form metal ion-PT/CeO_2 complexes. As described in Fig. 8, the result proposes that compared with Pb^{2+}, the other competitive metal ions only slightly quenched the fluorescence intensity of PT/CeO_2 due to the weak affinity between these metal ions and the interaction site of the developed probe. The main information in the selectivity test of the developed nanocomposite solution, the fluorescence emission of PT/CeO_2 is completely quenched by adding Pb^{2+} in the presence of other metal ions. Generally, other metal ions have a small influence on the selective detection of Pb^{2+}, this is due to the faster chelating process with the sensing site of PT/CeO_2 than the other metal ions.

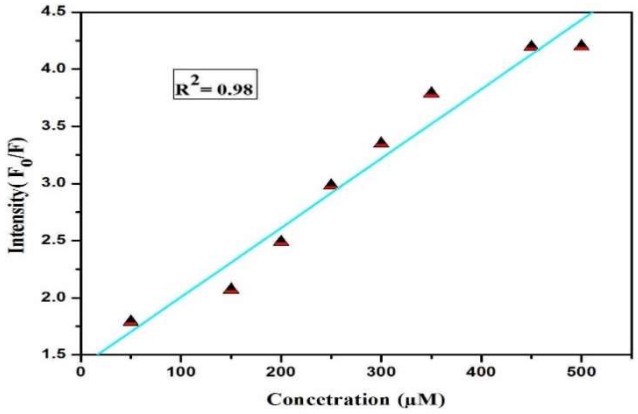

Fig. 7. The reproducibility of the PT/CeO_2 responses for Pb^{2+} concentration.

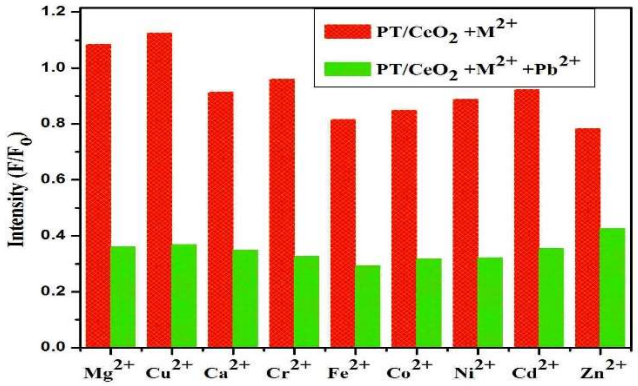

Fig. 8. Fluorescence responses of PB = PT/CeO_2 (left bar) after treatment of 0.5 mM metal ion solutions, and interference of 0.5 mM of other metal ions with 0.5 mM Pb^{2+} (right bar).

Recovery Test

88 tap water sample was spiked with different concentrations of Pb^{2+} solutions. The unknown concentration of Pb^{2+} in tap water is determined from the calibration curves plotted for the known standard solution (spiked) of Pb^{2+}, the unknown (found) concentration of Pb^{2+} (value of X) was successfully calculated by using equation y = A + B*X obtained from the calibration curves of the standard solution.

Where the value of "A" is intercept and B (slope) and the value of y (F_O/F) was obtained from the fluorescence recorded for Pb^{2+} from the spiked tap water sample. The result indicated a good linear relation between F_O/F and the spiked concentrations of Pb^{2+} with a coefficient of regression $R^2 = 0.99$ as designated in Fig. 9. The found values agreed well with the spiked amount. The obtained recoveries in such samples varied from 97.6 to 102.8% and the relative standard deviations (RSD) were less than 1% which indicates the developed sensor shows high validity and precision (Table 1).

Detection of Pb^{2+} in Real Samples

In this research, under optimizing all parameters, tap water samples contain a detectable amount of Pb^{2+} described in Fig. 10. Therefore, sulfur-containing polymer like polythiophene is a promising prospect for the detection of these toxic metal ions in real samples. The calculated amount of lead concentration in tap water was found to be 15.39 µM which is greater than the allowable limit of 0.01 mM as stated by WHO. This may be due to possible reasons for high levels of lead metal ions, lead was found in gasoline and house paint, which has been extended to lead water plumbing pipes. Hence, flow into water bodies and exposure to humans.

CONCLUSIONS

The polythiophene imprinted CeO_2 was synthesized by the polymerization method and the structural, and morphological behaviors were characterized by modern spectroscopy such as XRD, SEM, and FT-IR. The results of FT-IR and XRD analysis confirmed that there is a strong interaction between PT and CeO_2 nanocomposite. The developed fluorescent probe was utilized as a highly effective tool for the selective detection of Pb^{2+} ion. Consequently, with on addition of Pb^{2+} to PT/CeO_2, the emission intensity was decreased (quenched). Conducting polymer, particularly S- containing polythiophene shows a distinct fluorescent property for the detection of the lead metal ion. The operational parameter such as the effect of pH is evaluated with the range of 2-12, the result confirms a maximum quenching efficiency was observed at pH 7. The various concentrations of Pb^{2+} from 50-500 µM were tried to test the effect of concentration, linearity with $R^2 = 0.98$, and

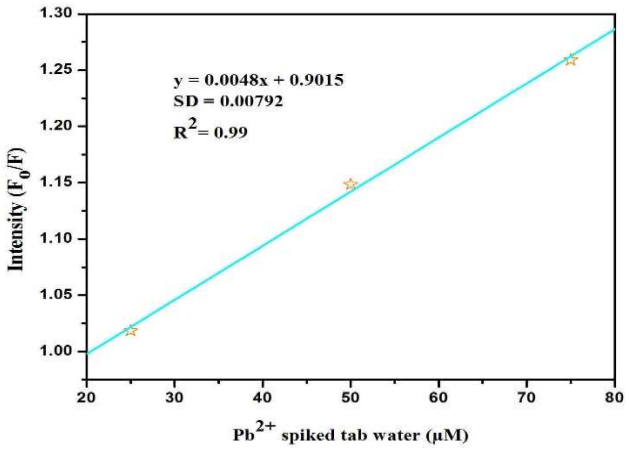

Fig. 9. Calibration curve of F_O/F *vs*. different concentration Pb^{2+} ions spiked samples.

Table 1. Detection of Pb^{2+} in Tap Water Samples by Spiked Method (n = 3)

Samples	Added (µM)	Found (µM)	Mean recovery (%)	RSD (%)
Tap water				
1	25	24.4	97.6	0.7
2	50	51.44	102.8	0.6
3	75	74.5	99.3	0.5
	Unknown	15.39		

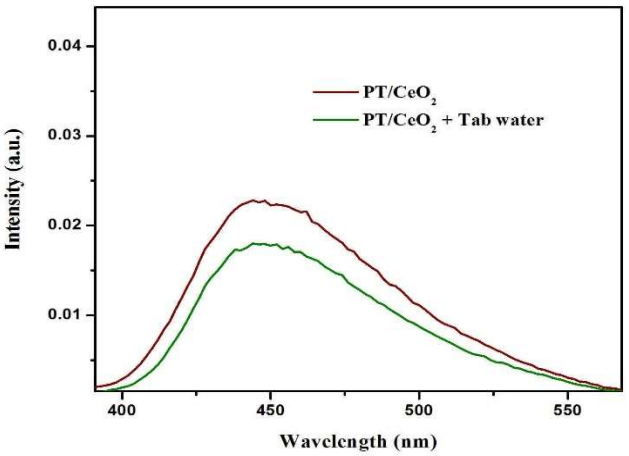

Fig. 10. Fluorescence emission spectra of PT/CeO_2 of the tap water samples.

sensitivity of the method. The newly developed probe exhibited a linear range, a high selectivity in the presence of other metal ions, and sensitivity with a low detection limit of 9.17×10^{-5} M.

ACKNOWLEDGMENTS

I thank my friend Getachew Asfaw for helping during laboratory work. I would like to express my deepest appreciation and thanks to the Department of Chemistry, Wollo university for the instruments and laboratory facilities. I would like also to thank Addis Ababa University for PL, XRD, and FT-IR analysis and the university of Taiwan university of science and technology for SEM analysis.

REFERENCES

[1] EPA, U.S. Environmental Protection Agency Report, EPA Washington, 2007.

[2] P.B. Tchounwou, C.G. Yedjou, A.K. Patlolla, D.J. Sutton, Molecular, Clinical and Enviro. Toxicol. (2012) 133.

[3] H. Ghrefat, N. Yusuf, Chemosphere, 65 (2006) 2114.

[4] U. Najeeb, W. Ahmad, M.H. Zia, Z. Malik, W. Zhou, Arab. J. Chem. 2014 (in press).

[5] W. Qihui, T. Qian, Procedia Engineering 18 (2011) 214.

[6] S. Morais, F.G. Costa, M.L. Pereira, Enviro. Health-Emerging Issues and Practice (2012) 227.

[7] S.J.S. Flora, M. Mittal, A. Mehta, I.J. Med. Res. 128 (2008) 501.

[8] I. Oehme, O.S. Wolfbeis, Microchimica Acta 126 (1997) 177.

[9] Z. Wang, L. Ma, Chem. Rev. 253 (2009) 1607.

[10] M. Faisal, S.B. Khan, M.M. Rahman, A. Jamal, K. Akhtar, M.M. Abdullah, J. Mate. Sci. & Technol. 27 (2011) 594.

[11] M. Palard, J. Balencie, A. Maguer, J.F. Hochepied, Mate. Chem. Phys. 120 (2010) 79.

[12] E. Sharpe, T. Frasco, D. Andreescu, S. Andreescu, Analyst 138 (2013) 249.

[13] N. Shehata, E. Samir, I. Kandas, Sensors 18 (2018) 2818.

[14] S. Wang, G.C. Bazan, Advan. Mater. 15 (2003) 1425.

[15] H.A. Ho, A. Najari, M. Leclerc, Accoun. Chemi. Rese, 41 (2008) 168.

[16] J.K. Mwaura, X. Zhao, H.J. Iang, K.S. Schanze, J.R. Reynolds, Chem. Mater. 18 (2006) 6109.

[17] A. Gogoi, C.K. Sarma, Mater. Chem. and Phys. 194 (2017) 327.

[18] J. Zhao, Y. Xie, Z. Le, J. Yu, Y. Gao, R. Zhong, Y. Qin, Y. Huang, Synthetic Metals 181 (2013) 110.

[19] K. Bisetty, M.I. Sabela, S. Khulu, M. Xhakaza, L. Ramsarup, Inter. J. Electrochem. 6 (2011) 3631.

[20] N.S. Alim, H.O. Lintang, L. Yuliati, J. Technol. (Sci. & Engin.), 76 (2015) 1.

[21] X.G. Li, J. Li, Q.K. Meng, M.R. Huang, J. Phys. Chem. B 113 (2009) 9718.

[22] M. Zawadzki, Journal of Alloys Compounds 454 (2008) 347.

[23] D. Kelkar, A. Chourasia, J. Chem & Chemi Technol. 5 (2011) 3.

[24] C. He, W. Zhu, Y. Xu, T. Chen, X. Qian, Analytica Chimica Acta 651 (2009) 227.